FRICTION CHARACTERISTICS OF MICROTEXTURED SURFACES UNDER HYDRODYNAMIC LUBRICATION

BY

ASHWIN RAMESH

THESIS

Submitted in partial fulfillment of the requirements
for the degree of Master of Science in Mechanical Engineering
in the Graduate College of the
University of Illinois at Urbana-Champaign, 2012

Urbana, Illinois

Adviser:

Prof. William Paul King

ABSTRACT

Surface microtexturing has shown significant promise over the past decade as one of the surface engineering methods to modify friction performance. We tackle two important problems associated with surface texturing – developing low cost scalable manufacturing technique and engineering design rules for fluid power applications. We report experimental and numerical investigation of the friction characteristics of microtextured surfaces. The textures are of size 28-257 μm on stainless steel surfaces, fabricated using micro-casting. Friction characteristics of these surfaces were tested under submerged condition using a pin-on-disk configuration. Numerical simulations solved the Navier-Stokes equations to predict the texture-induced lift. During hydrodynamic lubricated sliding, the textured surfaces exhibit friction as much as 80% lower than the untextured surfaces. We study the effect of operating conditions on the friction performance of the surfaces for different textures. The trends obtained in the experiments match well with the simulations, and indicate design rules for the implementation of this technology.

Keywords: Surface engineering, microtexturing, hydrodynamic lubrication, texture, Navier-Stokes

This thesis is dedicated to my family, colleagues and friends.

ACKNOWLEDGMENTS

I would like to thank my parents and my brother, who have always been a pillar of strength and for their unflinching support at all times, without whom I will not be who I am today.

I also take this opportunity to express my gratitude to my advisor Professor William Paul King, not only for giving me support, guidance and the opportunity to work on this project but also for helping me develop my presentation and communication skills and for helping me grow professionally.

Special thanks to my colleagues and friends for their constant support and motivation throughout the course of my Master's program. Special thanks to Wasim Akram, Suryapratap Mishra, Andrew Cannon and Prof. Andreas Polycarpou for their help and advice during the project. Thanks to Suhas, Matt, James, Sezer and Mohith for the intellectual discussions and for the great time I had at Champaign-Urbana.

I would like to extend my thanks to the National Science Foundation (NSF) and the Center for Compact and Efficient Fluid Power (CCEFP) in particular for financially supporting my work and for providing me the opportunity to discuss and interact with great minds around the country.

TABLE OF CONTENTS

CHAPTER 1: INTRODUCTION

The presence of micrometer-scale textures on a surface can modify the friction characteristics of that surface. It has long been known that micrometer-scale surface irregularities affect the load capacity of parallel sliding surfaces [1], however only recently have such textures been engineered to improve friction performance of mechanical parts [2, 3]. Microtextures act as microhydrodynamic bearings, enhancing load support and increasing film thickness, which leads to lower friction compared to untextured surfaces. Recent research has considered optimization of micro-dimples for automotive components including bearings and piston rings [4-6]. These studies highlighted the importance of dimple depth and its impact on reducing the friction coefficient. Other research has shown that micrometer-scale roughness orientation plays a key role in friction characteristics [7]. The packing density of the textures also affect friction [8].

Several published articles use computational fluid dynamics to study lubricant flow over micrometer-scale textures [2, 3, 6-14]. In some cases, textured surfaces in hydrodynamic lubrication can be accurately modeled by the Reynolds equation. However the Reynolds equation is not accurate when inertial effects are important when the Reynolds number is high, Re ~ >8, when the textures have high depth to width ratio, or when the film thickness is larger than the texture depth [9-12]. Few articles have reported that the Navier-Stokes equations must be solved in order to account for the role of convective inertia in generating lift from surface textures [13, 14]. In order to broadly investigate many geometries and operating conditions, this thesis solves the full Navier-Stokes equations in two dimensions.

A key technical challenge to realizing microtextured surfaces in industrial applications has been the lack of micro-manufacturing technologies that can form friction-reducing surface

microtextures at large scales and in real engineering materials. Surface texturing techniques for tribological applications include chemical etching, shot blasting, ion beam etching, photolithography and laser texturing [3, 15-24]. Some published reports investigate sliding friction on micro-structured semiconductor surfaces [15, 16], which are too brittle for industrial applications and cannot be scaled beyond several inches. It is possible to fabricate microtextured steel using photolithography and chemical etching [17], but this approach is not easily scaled to substrates with complex three-dimensional shapes. Finally, laser texturing has been considered for manufacturing micro-textures [3, 18-21], but it has relatively low throughput and has limits on the textures that can be produced.

This thesis describes experimental and numerical investigation of lubricated sliding surfaces having micro-scale surface textures. A micro-casting process that can be scaled to curved surfaces and large areas is applied to produce micro-textures on stainless steel surfaces and tested under unidirectional pin-on-disk configuration using a tribometer. We solve the full Navier-Stokes equations to compare with trends obtained from the experiments under hydrodynamic conditions.

Table 1.1 summarizes the key literature in the experimental investigation of microtextured surfaces for friction reduction. The table lists the textures tested, the operating conditions used and the manufacturing methodology used to produce these microscale textures. Table 1.2 highlights the key literature in the numerical study of microtextured surfaces. Key parameters like texture geometry, operating conditions and the numerical model are listed. Conclusions drawn in terms of the optimum texture parameters for these conditions are also listed in the table.

Table 1.1. Summary of literature in the experimental domain and the key parameters studied

Author	Regime	Texture width (µm)	Texture depth (µm)	Lubricant	Viscosity @20 °C (Pa.s)	Pressure (MPa)	Velocity (m/s)	Textured material	Texture method
Geiger (1998)	HD, EHL	25 -- 150	5 -- 20	Mineral oil	1.5		1 -- 2	Ceramic	LST
Dumitru (2000)	HD, BL	5 – 10	5 – 8	Mineral oil	0.096 @40 °C		0.01	440 Stainless	LST
Ryk (2002)	HD	100	8 -11, 19, 20	SAE 40	0.113 @40 °C	0.1 - 0.5		Chrome coated steel	LST
Wang (2003)	HD	50 - 650	2 - 16.6	Water	0.001	1.5 - 15	0.31 -- 0.94	SiC	RIE
Pettersson (2003)	BL	5, 20, 50	5	Poly-alpha olefin		680	0.0125	TiN, DLC on Si	PL and KOH etch
Pettersson (2004)	BL	5, 20, 50	5	Poly-alpha olefin		680	0.0125	DLC on Si	PL and KOH etch
Kovalchenko (2004)	BL – HD	58 - 140	4 – 6.5	10W30 15W50	0.047, 0.11 @40 °C	0.16 – 1.6	0.15 – 0.75	52100 steel	LST
Nakano (2007)	HD	60, 500	6 - 10, 45 - 50	VG 68	0.059	1, 6	0.083 - 1.0	Cast iron	Shot blasting
Pettersson (2007)	BL	5 -- 20		Mineral oil	0.02	100	0.006	Steel	Embossing
Costa (2007)	HD	40 - 130	1.8 - 8	Mineral oil	1.5	9.4 - 24.1	0.0121	Steel	PL and chemical etch
Nakano (2009)	HD	30 - 40	10 -- 12	VG 32, 68, 320	0.026 – 0.27	0.014 - 0.14	0.001 - 0.005	NiFe on Si	PL and DRIE
Qiu (2011)	HD	250 - 2000	46 - 60	SAE 30 engine oil			0.05 - 4.2	17-4PH stainless	LST
Yamakiri (2011)	BL	11 -- 35	8 -- 24	Water	0.001	0.1 - 0.8	0.042 - 0.25	Si_3N_4	LST
Surya (2011)	BL	40 – 60	4 – 10	PAG, POE	0.06	5.71	0.96 – 3.84	Cast iron	LST
Mitchell (2012)	HD	10 - 100	5 -- 60	N35 mineral oil	0.06		0.01	316L stainless	µ-casting

HD – Hydrodynamic lubrication; EHL – Elasto-hydrodynamic lubrication; BL – Boundary lubrication; DLC – Diamond like carbon; LST – Laser surface texturing; RIE – Reactive ion etching; PL – Photolithography; KOH – Potassium hydroxide; DRIE – Deep reactive ion etching; PAG – Polyalkylene glycol; POE – Polyol ester; VG – Viscosity grade

Table 1.2. Summary of literature in the numerical domain and the key parameters studied

Author	Regime	Model	Texture geometry	Optimum texture parameters	Viscosity (Pa.s)	Pressure (MPa)	Velocity (m/s)	Application
Etsion (1996)	HD	Reynolds	Hemispherical dimples	Width: 10 – 20 µm Area density: 20 %	0.001	0.5 – 3	9.5	Mechanical seals
Ai (1996)	EHL	Reynolds	Transverse, longitudinal, oblique roughness	Transverse and longitudinal roughness perform well	0.04	230 – 380		High pressure seals
Ronen (2001)	HD	Reynolds	Spherical dimples	Depth over diameter ratio: 0.1 – 0.18 Area density: 5 – 20 %				Reciprocating automotive
Arghir (2003)	HD	NS	Rectangular, Sinusoidal, Triangular C/S		Re: 0.1-100			Various applications
Siripuram (2004)	HD	Reynolds	Circle, Square, Diamond, Hex, Triangle	+asperities: Area density: 0.2 – 0.3 -asperities: Area density: 0.4 - 0.5	0.042	0.1	2.66	Mechanical seal
Sahlin (2005)	HD	NS	Cylindrical, splined C/S	Depth to FT ratio: 0.5 – 0.75 High area density	Re: 40 - 160			Various applications
Brajdic (2005)	HD	NS	Square pockets	Depth to FT ratio: ~20	0.009	0.5 - 50	1	Pad bearing
Kligerman (2005)	HD	Reynolds	Partial textures with spherical dimples	Textured portion: 60 % High area density Aspect ratio: 0.1 Depth: 10 – 20 µm	0.083	0.4	4.8	Piston rings
Dobrica (2009)	HD	Reynolds and NS	Square pockets	Discusses applicability of Reynolds equation	Re: 0.125 – 256			Various applications
Dobrica (2010)	HD	Reynolds	Trapezoidal textures – Partial and full	High area density Depth to FT ratio: 0.4 – 0.8	0.03	FT = 15 µm	5	Pad bearing
Han (2010)	HD	NS	Spherical dimple	Depth to FT ratio: 0.8 – 2 High area density	Re: 10 – 160			Various applications
Qiu (2011)	HD	Reynolds	Spherical dimple	Predicts optimum dimple density, depth and depth to diameter ratio	0.0002 – 1	FT = 2 – 24 µm	0.63 – 3.77	Thrust bearing, mechanical seal

HD – Hydrodynamic lubrication; EHL – Elasto hydrodynamic lubrication; NS – Navier-Stokes; FT – Film thickness; Re – Reynolds number; C/S – cross-section

CHAPTER 2: EXPERIMENTAL

2.1 Experimental setup

Unidirectional sliding tests were performed on a High Pressure Tribometer (HPT) between a stationary nominally flat textured pin and a rotating untextured disc with constant applied normal load (N) and rotational velocity (u). A 6-axis strain gage load cell measured the in-situ friction and normal forces between the surfaces, which was then used to calculate the friction coefficient. Further technical details and schematic of the test rig can be found in literature [25, 26]. The pin and disc were immersed in a pool of lubricant (submerged conditions) but otherwise the system was maintained at room temperature and atmospheric pressure. The lubricant used was 85W-140 gear oil with a viscosity (η) of 1.5 Pa.s at 20^{o}C. We selected this lubricant for its technical relevance, as it is used in many automotive and pump applications. While the oil has some additives, we note that the same oil type was used for all measurements and so the measurements fairly compare textured vs. nontextured surfaces for real applications.

2.2 Experiment methodology

Table 2.1 lists the samples fabricated and their texture geometry. The samples were chosen such that the effect of geometrical parameter like texture width, depth and density is studied independently. Prior to the tests, the samples were screened using an optical microscope to ensure that the inclination of the specimen was less than 5 µm over a 6.3 mm length; 5 µm was chosen since the average peak-peak of the roughness of the pins was 5 µm. This was done to ensure that surface inclination does not contribute to the load. The samples were subsequently cleaned in a pool of acetone for 10 minutes in ultrasound followed by rinsing with isopropyl

alcohol. An initial preload of 45 N was applied to the pin for 10 seconds before the tests in order to further ensure conformal contact of the pin and the disc. Each test was 30 minutes, and the steady state friction coefficient was calculated as the average of the friction coefficient after 15 minutes of testing. The mass of the pin and the disc were measured before and after the tests to quantify wear, if any, during the experiments. Repeatability tests were performed for the samples to ensure parallelism of the contacting surfaces. Good match between repeat tests showed that surface inclination was not a factor in the load support for the specimens. Moreover, the width of the burnishing tracks on the disc due to run-in effects were quantified after the tests and an average track width of 6.0 mm for the tests confirmed conformal contact between the surfaces considering that the pin is cylindrical with circular cross-section.

Table 2.1. List of Samples and Pattern Geometry.

Pattern	Feature shape	Width (μm)	Depth (μm)	Pitch (μm)	Density (%)	Aspect ratio (Depth/Width)
A	-	0	0	0	0	-
B	Square	28	42	44	31.8	1.50
C	Circle	32	30	53	28.6	0.94
D	Circle	74	42	131	25.1	0.57
E	Circle	101	32	257	12.1	0.32
F	Circle	102	36	182	24.7	0.35
G	Circle	97	26	140	37.7	0.27
H	Circle	101	65	174	26.5	0.64
I	Circle	113	105	183	29.9	0.93
J	Circle	109	133	182	28.2	1.22

2.3 Textured sample

The pins were made of 17-4 PH stainless steel and the discs were made of 304 stainless steel. The pin diameter was 6.3 mm and the disk diameter was 76 mm. The RMS surface roughness (R_q) of the pins was 0.36 µm before the tests and that of the discs was 0.11 µm. The micro-textured pins were fabricated by a micro-casting process described in the literature [27, 28]. Figure 2.1 shows a photograph of the stainless steel pin and a Scanning Electron Microscope image of the microtextures. An important characteristic of these textures is the absence of material pile-up around the circumference of the dimples that are typical of laser surface texturing methods [19, 29]. The absence of this pile-up provides a textured surface well suited to the present application of drag reduction.

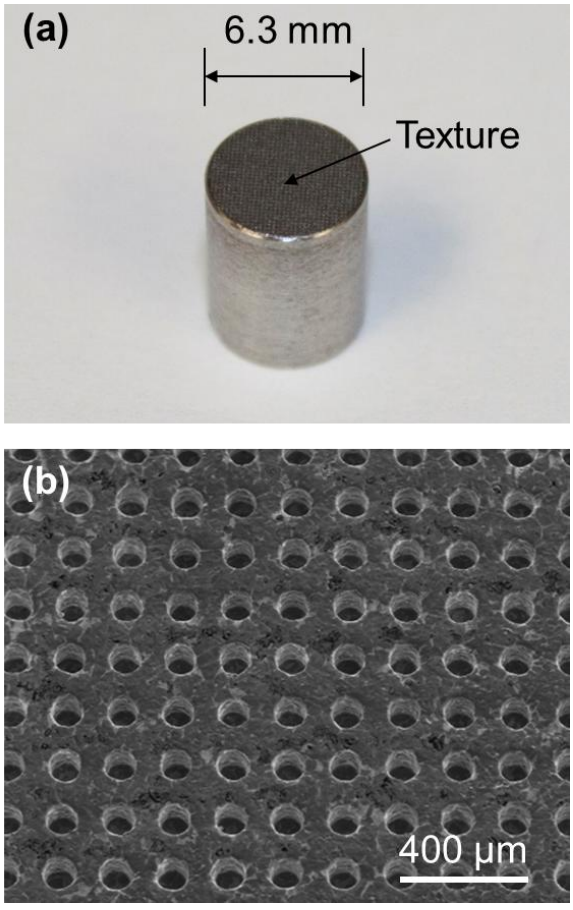

Figure 2.1 (a) Textured stainless steel pin J and (b) SEM image highlighting the textures.

CHAPTER 3: SIMULATION

3.1 Problem setup

Figure 3.1a shows the simulation cell highlighting the texture geometry and the boundary conditions.

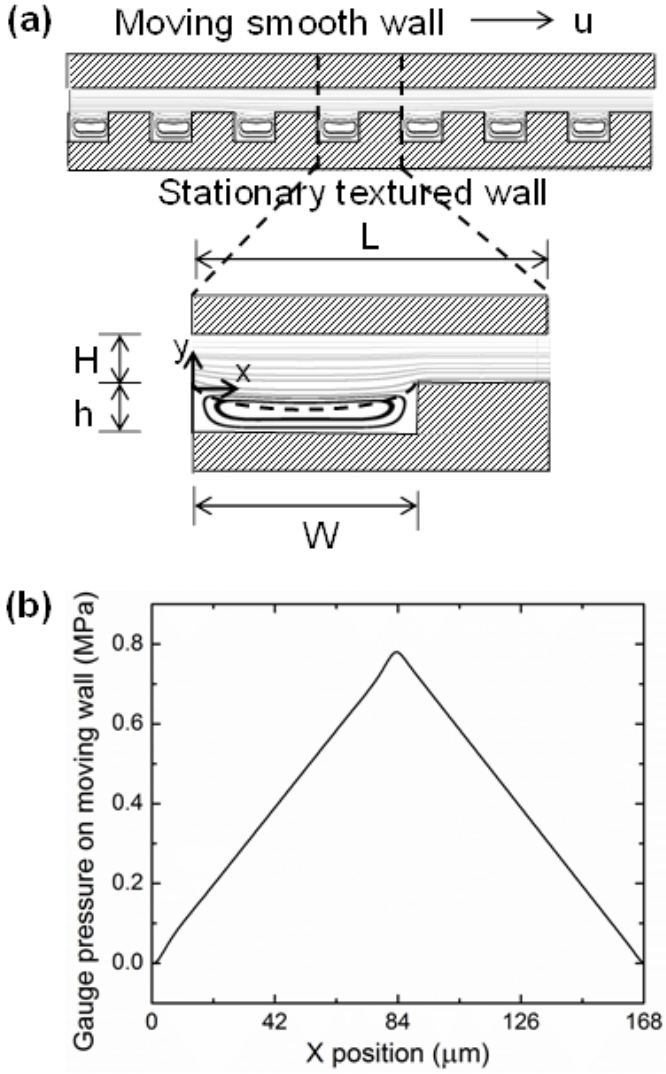

Figure 3.1: (a) Schematic of a computational cell with a moving smooth wall against a stationary textured wall with inlet textures, showing key geometry. (b) Prediction for pressure on top wall.

In order to reduce the complexity involved in modeling three dimensional geometries we use a 2D computational domain with the texture being a cylinder in cross-section. Previous research has shown that the pressure profiles for 3D and 2D texture geometries are similar and we could fairly accurately predict the load using a 2D geometry [13] [14] [30]. We found that the computational results are the same regardless of where the texture is placed within the computational domain.

The fluid is modeled as isoviscous, isothermal, and constant density. We assume steady-state conditions with periodic boundary conditions and zero gauge pressure on either end. The untextured top wall moves with a constant velocity (u) and the textured bottom wall is stationary. A computational fluid dynamics code, FLUENT®, solves the Navier-Stokes equations. The governing equations are

$$\boldsymbol{\nabla}.\boldsymbol{u} = 0 \tag{1}$$

$$\rho(\boldsymbol{u}.\boldsymbol{\nabla}\boldsymbol{u}) = -\boldsymbol{\nabla}p + \eta\nabla^2\boldsymbol{u} \tag{2}$$

where $\boldsymbol{u}$ is the velocity vector, p is the pressure, ρ is the fluid density and η is the viscosity. We used first order upwind scheme for momentum discretization and standard scheme for pressure discretization. The algorithm used in the simulations decoupled pressure and velocity [32]. The convergence criterion was 10^{-7} for the residuals of all the governing equations. The input parameters were texture geometry and fluid properties and the simulation outputs were shear stress and hydrodynamic pressure on the top wall.

A wide range of parameters were studied with texture width (W) varying from 20 - 1000 μm, texture depth (h) 1 - 100 μm and texture density ($\gamma = \frac{\pi}{4}\frac{W^2}{L^2}$) 4 - 63%. Figure 3.1b shows the pressure profile on the top wall for u = 0.36 m/s and η = 1.5 Pa.s for a texture with W = 84 μm, L = 168 μm, h = 10 μm. The pressure profile is linear similar to Rayleigh step bearings [31, 33,

34]. We kept the pressure (P) on the top wall constant in order to find the film thickness for this applied load. The relationship between applied load and film thickness was the same, regardless of which one was held constant.

3.2 Simulation results

Figure 3.2 shows the predicted non-dimensional friction force as a function of texture parameters at constant load. We define the non-dimensional friction force (F^*) as the ratio of the friction force (F) to atmospheric pressure (p_a) times the area (A), $F^* = F/(p_a A)$. The friction force is minimum when the texture depth is approximately equal to the film thickness (Fig. 3.2a). This critical texture depth depends on the load and decreases with increasing load. Friction force decreases with increasing texture density (Fig. 3.2b) and width (Fig. 3.2c). However, beyond a texture density of about 30% and a width of about 200 μm, the reduction in friction force is somewhat lower. For the constant load applications studied here, we identify good performance for texture with $h \sim H$, $\gamma \sim$ 20 - 30% and $W \sim$ 100 – 200 μm.

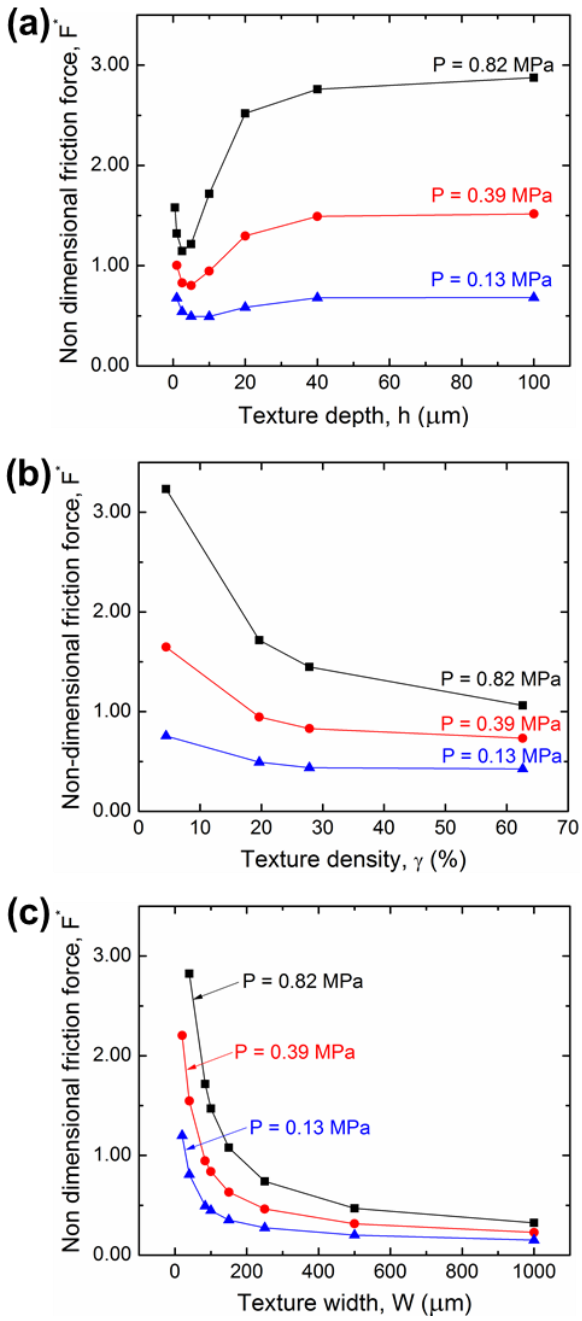

Figure 3.2: Prediction for non-dimensional friction force as a function of texture parameters for u = 0.36 m/s and η = 1.5 Pa.s at constant load. (a) Texture depth dependence for texture density γ = 20 % and pitch L = 168 μm. (b) Texture density dependence for texture depth h = 10 μm and pitch L = 168 μm. (c) Texture width dependence for texture depth h = 10 μm and density γ = 20 %.

CHAPTER 4: RESULTS AND DISCUSSION

Table 4.1 summarizes the different operating conditions used in the experiments and the average measured friction coefficient values. The range of N was 125 - 254 N and the range of u was 0.36 - 0.6 m/s. The corresponding range of contact pressures was 4 – 8.1 MPa.

Table 4.1: List of experiments and measured friction coefficients.

Pattern	Normal load (N)	Contact pressure (MPa)	Sliding Velocity (m/s)	Average steady State COF
A	151	4.84	0.36	0.051
B	151	4.84	0.36	0.048
C	151	4.84	0.36	0.053
D	151	4.84	0.36	0.036
E	151	4.84	0.36	0.074
F	151	4.84	0.36	0.032
G	151	4.84	0.36	0.028
H	151	4.84	0.36	0.019
I	151	4.84	0.36	0.008
J	151	4.84	0.36	0.028
B	125	4.01	0.48	0.178
F	125	4.01	0.48	0.142
F	125	4.01	0.6	0.112
H	125	4.01	0.6	0.149
A	171	5.49	0.36	0.026
B	171	5.49	0.36	0.033
F	171	5.49	0.36	0.026
A	254	8.15	0.36	0.126
H	254	8.15	0.36	0.097

At a given operating condition, the textured samples generally have lower friction coefficient compared to untextured sample. This friction reduction can be attributed to the added hydrodynamic load support provided by the textures thereby increasing the film thickness and reducing friction. A few of the samples, B, C and E, have higher friction coefficient than the untextured sample. Samples B and C have low texture width and sample E has low texture density. From Fig. 3.2, friction increases significantly with decreases in texture width and density.

Figure 4.1 shows Scanning Electron Microscope (SEM) images of the textured and untextured samples before and after testing. Comparison of the untextured sample images before and after testing showed minor scratches consistent with metal to metal contact (Fig. 4.1a-4.1b). However no wear could be quantified, indicating that the burnishing only occurred. Note that under submerged conditions one is not expecting significant contact, yet the load/speed was such that asperity contact was sustained, indicating mixed lubrication. Comparison of the images of the textured sample F before and after the experiment (Fig. 4.1c-4.1d) showed no visible scratches, indicating that the pin did not make contact with the disk. This was expected, as the textured surface should have increased the load carrying capacity compared to the smooth surface, leading to hydrodynamic (full film) lubrication for the textured surface [2, 13, 35].

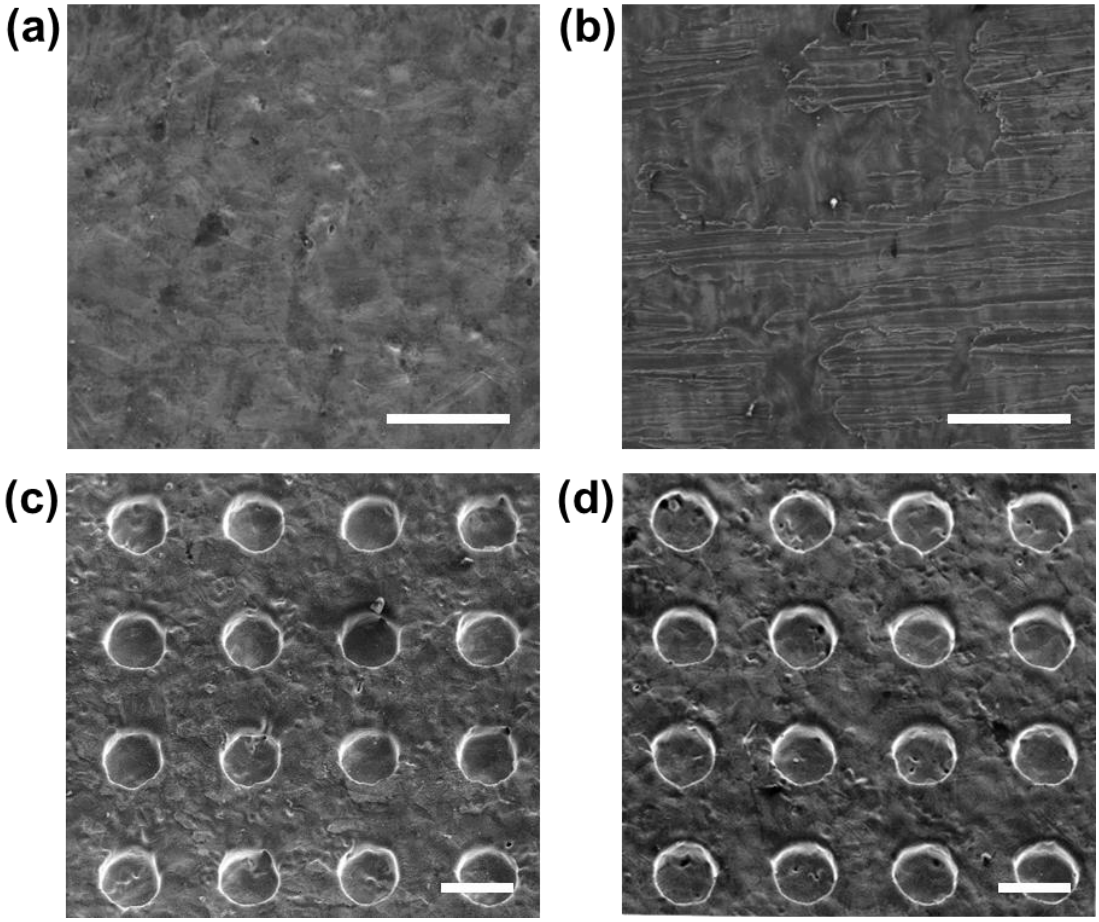

Figure 4.1: Scanning Electron Microscope (SEM) images of untextured sample A (a) before and (b) after the experiment at N = 151 N, u = 0.36 m/s and η = 1.5 Pa.s. The pin experienced some scratches during the test indicating metal to metal contact. SEM images of textured sample F (c) before and (d) after the experiment. Almost no wear is visible on the textured pin. Scale bar in the images represent 100 µm.

Figure 4.2a shows the friction coefficient as a function of sliding distance for samples A (untextured), F, and H. All of the textured samples had similarly stable friction coefficient with the exception of sample I. All of the samples, including sample I, showed no visible wear. Surface texturing enhances the load carrying capacity and provides a stable load support, which is consistent with previous reports [22, 23].

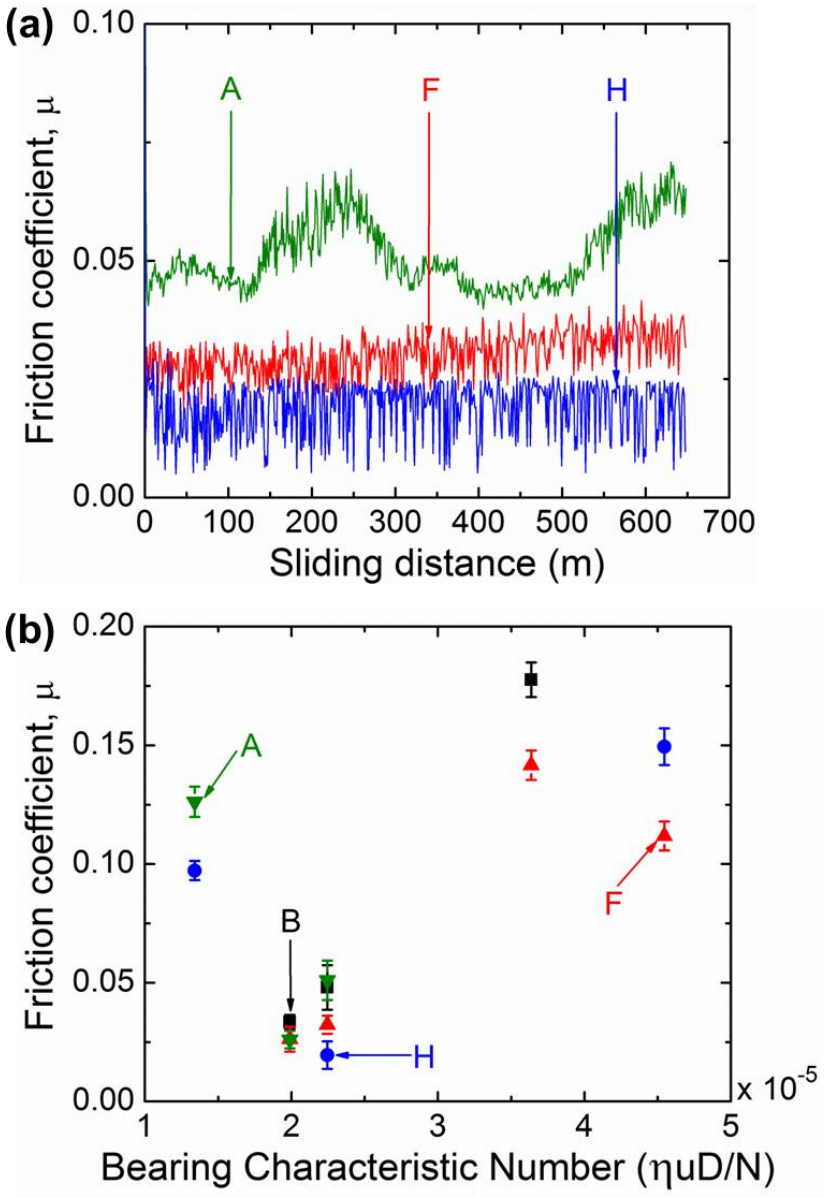

Figure 4.2: (a) Friction coefficient with sliding distance for three samples for N = 151 N, u = 0.36 m/s and η = 1.5 Pa.s. (b) Friction coefficient as a function of bearing characteristic number.

Figure 4.2b shows friction coefficient variation with bearing characteristic number for several textured and untextured surfaces. The bearing characteristic number is a nondimensional number that can identify the regime of lubrication $B = \eta uD/N$ where D is pin diameter. The friction coefficient decreases with B until $B = 2 \times 10^{-5}$. Beyond this, the friction coefficient increases with B, a trend characteristic of hydrodynamic lubrication. While the measured

friction coefficients at high bearing characteristic numbers are high for the full film regime, there was no observable wear in these specimens. Moreover, the friction coefficient evolution for these specimens shows a stable trend indicating a stable hydrodynamic load. The full film regime is also expected since the film thicknesses predicted for these conditions are greater than three times the RMS surface roughness of the pins [36]. The remainder of the thesis discusses the effect of texture geometry in the hydrodynamic regime at B = 2.25 x 10^{-5}. Also, from Fig. 4.2b, the texture geometry with the lowest friction varies with the operating conditions, in accordance with the predictions and literature [2, 14]. Hence, the experimental results obtained in the subsequent section identifying texture geometry with low friction is specific to B = 2.25 x 10^{-5}.

The friction force on the textured surfaces can be expressed as

$$F = \eta A u \left(\frac{1-\gamma}{H} + \frac{\gamma}{H_{eff}} \right) \tag{3}$$

where the effective film thickness in the textured region $H_{eff} = f(H, h, W)$. Due to fluid recirculation within the cylindrical dimples, there is a zone where the fluid velocity is zero, highlighted by the dashed line in Fig. 3.1a. The height of this zone is approximately half the texture depth (h/2) and the width is W. The volume of fluid that is sheared in the textured region is the sum of volume of the fluid in a cylindrical region of height H and width W and that of the fluid within the zero velocity zone with height h/2 and width W. In order to find an approximate expression for H_{eff}, we equate this total volume to that of the fluid that is sheared in an equivalent cylindrical section with height H_{eff} and width W. This leads to the following expression for H_{eff}.

$$H_{eff} = H + \frac{h}{12}(3 + \lambda^2); \tag{4}$$

where $\lambda = \frac{h}{W}$ is the aspect ratio. The film thickness in the experiments was estimated using eqn. 3 and eqn. 4 and the experimentally obtained friction force. The simulations used this film thickness to predict the friction force and load to compare with the experiments.

Figure 4.3 shows experimental and predicted friction force as a function of texture parameters. There is overall very good agreement between experiments and predictions. From Fig. 4.3a, friction force attains a minimum at a particular texture depth, which is consistent with the trend in Fig. 3.2a and predictions in the literature [2, 14]. For these experimental conditions, this minimum is attained at a texture depth of 105 μm. Figure 4.3b shows the effect of texture density on the friction force between sliding surfaces. Friction decreases with increasing texture density; however, beyond a density of 25%, the friction force reduction is small which is in accordance with the predictions of Fig. 3.2b. From Fig. 4.3c, friction force decreases with increase in texture width. However, there is a critical width beyond which there is only a small change in friction; a trend similar to Fig. 3.2c. For these conditions this critical width is about 102 μm.

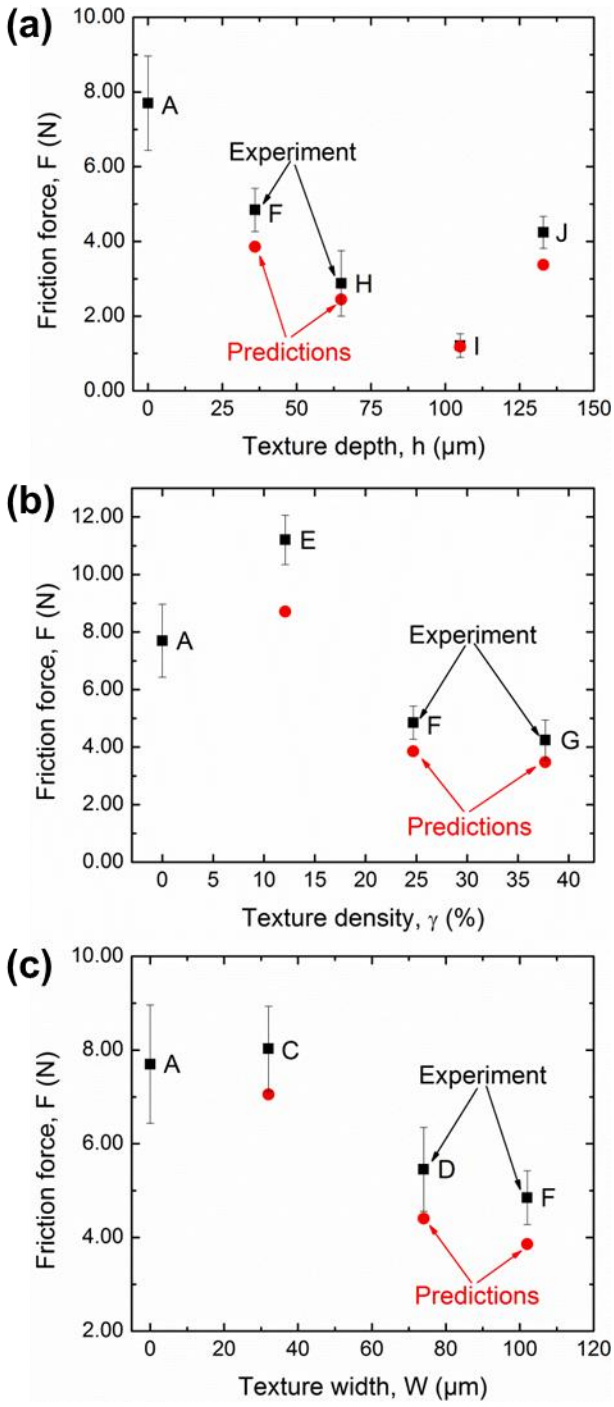

Figure 4.3: Experimental and predicted friction force for N = 151 N, u = 0.36 m/s and η = 1.5 Pa.s. (a) Effect of texture depth (b) Effect of texture density (c) Effect of texture width.

We have demonstrated the ability of the current manufacturing process to produce a wide range of textured samples and samples without material pile-up to prevent metal-metal contact and provide low fluid drag, thus low friction. The experimental and numerical results are important from the point of view of designing optimal textures for various applications. We find a good agreement between the experimental results (Fig. 4.3) and numerical predictions (Fig. 3.2). In order to obtain accurate predictions of the optimal texture geometries, numerical models must take into account the inertial contribution of the textures to the increased lift. Several other factors like roughness and waviness of the samples also play an important role in the prediction of load carrying capacity [1, 37, 38]. These factors are not included in this model and hence the absolute values of the load predicted from the simulations were lower than the experimental load applied for these conditions. An accurate numerical model solving the Navier-Stokes equations which also includes these additional factors could be a subject of further research.

CHAPTER 5: CONCLUSIONS

5.1 Summary

We have applied a low cost scalable manufacturing technique to produce microtextures on stainless steel surfaces to enhance the friction performance. We report friction reduction as high as 80% for textured surfaces compared to untextured surfaces through experiments for these operating conditions. The simulations predict texture geometries for constant load applications that lead to low friction. We have experimentally validated these trends, allowing suitable texture geometry prediction for various applications. For constant load applications, we identify the texture with $h \sim H$, $\gamma \sim$ 20 - 30% and $W \sim$ 100 – 200 μm as the texture with good friction performance. Microtextured surfaces can find application in fluid power systems like seals, pumps and valves to significantly reduce friction and wear in these systems.

5.2 Future work

5.2.1 Constant clearance experiments

Constant clearance applications are typical of some fluid power and automotive systems. Valves sliding within bearings, piston rings sliding within a casing, etc. are examples of constant clearance applications where it is important to understand the effect of surface texturing on the friction and load between the surfaces. Some numerical results for such applications are presented in the appendix section of this thesis (A.1). It is difficult to perform displacement controlled sliding tests and hence, there is no literature for such tests. For this, we will be collaborating with Prof. Randy Ewoldt of the Mechanical Science and Engineering department at University of Illinois – Urbana Champaign. We will perform constant clearance tests in a

rheometer that has the capability to measure the shear torque and the normal load when two surfaces rotate relative to one another. Experiments will be performed at different clearances and with different fluids. The effect of textures on the shear rate and consequently the viscosity of Non-Newtonian fluids will also be studied both experimentally and numerically.

5.2.2 Scuffing tests

Surface texturing enhances the friction performance for refrigeration and air-conditioning applications [29]. The textures used in the study, produced by laser surface texturing, had material pile-up around the dimple leading to metal – metal contact during initial sliding and hence, high friction. The textures produced by the micro-casting process mentioned above do not have material pile-up and hence, would be beneficial for such applications. Future work will focus on testing these textures in applications relevant to refrigeration and air-conditioning. The aim will be to compare the tribological performance of untextured and textured interfaces in the boundary lubrication regime. A specific type of test called scuffing test will be performed to simulate contact in compressors. The normal load on the samples will be increased with time and the maximum load that the interface can withstand before failure will be analyzed. This process of failure, where the friction coefficient increases drastically is called scuffing. Textured interfaces are anticipated to increase the scuffing time and also the normal load that the interface can withstand. Such tests will be performed in the presence of HFO-1234yf refrigerant both with and without Polyalkelyne glycol (PAG) lubricant. The sliding speeds will be in the order of 2 – 3 m/s with the load increased by 40 – 50 N/min.

REFERENCES

[1] Hamilton DB, Walowit JA, Allen CM. A Theory of Lubrication by Micro-Irregularities. Journal of Basic Engineering. 1966;88:177-&.

[2] Etsion I, Burstein L. A model for mechanical seals with regular microsurface structure. Tribol T. 1996;39:677-83.

[3] Etsion I, Kligerman Y, Halperin G. Analytical and experimental investigation of laser-textured mechanical seal faces. Tribol T. 1999;42:511-6.

[4] Ronen A, Etsion I, Kligerman Y. Friction-reducing surface-texturing in reciprocating automotive components. Tribol T. 2001;44:359-66.

[5] Brizmer V, Kligerman Y, Etsion I. A laser surface textured parallel thrust bearing. Tribol T. 2003;46:397-403.

[6] Kligerman Y, Etsion I, Shinkarenko A. Improving tribological performance of piston rings by partial surface texturing. J Tribol-T Asme. 2005;127:632-8.

[7] Ai XL, Cheng HS. The effects of surface texture on EHL point contacts. J Tribol-T Asme. 1996;118:59-66.

[8] Wang QJ, Zhu D. Virtual texturing: Modeling the performance of lubricated contacts of engineered surfaces. J Tribol-T Asme. 2005;127:722-8.

[9] de Kraker A, van Ostayen RAJ, van Beek A, Rixen DJ. A multiscale method modeling surface texture effects. J Tribol-T Asme. 2007;129:221-30.

[10] Dobrica MB, Fillon M. About the validity of Reynolds equation and inertia effects in textured sliders of infinite width. P I Mech Eng J-J Eng. 2009;223:69-78.

[11] Han J, Fang L, Sun J, Wang Y, Ge S, Zhu H. Hydrodynamic Lubrication of Surfaces with Asymmetric Microdimple. Tribol T. 2011;54:607-15.

[12] Li J, Chen HS. Evaluation on applicability of reynolds equation for squared transverse roughness compared to CFD. J Tribol-T Asme. 2007;129:963-7.

[13] Arghir M, Roucou N, Helene M, Frene J. Theoretical analysis of the incompressible laminar flow in a macro-roughness cell. J Tribol-T Asme. 2003;125:309-18.

[14] Sahlin F, Glavatskih SB, Almqvist T, Larsson R. Two-dimensional CFD-analysis of micro-patterned surfaces in hydrodynamic lubrication. J Tribol-T Asme. 2005;127:96-102.

[15] Nakano M, Miyake K, Korenaga A, Sasaki S, Ando Y. Tribological Properties of Patterned NiFe-Covered Si Surfaces. Tribol Lett. 2009;35:133-9.

[16] Siripuram RB, Stephens LS. Effect of deterministic asperity geometry on hydrodynamic lubrication. J Tribol-T Asme. 2004;126:527-34.

[17] Costa HL, Hutchings IM. Hydrodynamic lubrication of textured steel surfaces under reciprocating sliding conditions. Tribology International. 2007;40:1227-38.

[18] Geiger M, Roth S, Becker W. Influence of laser-produced microstructures on the tribological behaviour of ceramics. Surface & Coatings Technology. 1998;100:17-22.

[19] Dumitru G, Romano V, Weber HP, Haefke H, Gerbig Y, Pfluger E. Laser microstructuring of steel surfaces for tribological applications. Applied Physics a-Materials Science & Processing. 2000;70:485-7.

[20] Wang XL, Kato K, Adachi K, Aizawa K. The effect of laser texturing of SiC surface on the critical load for transition of water lubrication mode from hydrodynamic to mixed. Tribology International. 2001;34:703-11.

[21] Andersson P, Koskinen J, Varjus S, Gerbig Y, Haefke H, Georgiou S, et al. Microlubrication effect by laser-textured steel surfaces. Wear. 2007;262:369-79.

[22] Pettersson U, Jacobson S. Friction and wear properties of micro textured DLC coated surfaces in boundary lubricated sliding. Tribol Lett. 2004;17:553-9.

[23] Nakano M, Korenaga A, Korenaga A, Miyake K, Murakami T, Ando Y, et al. Applying micro-texture to cast iron surfaces to reduce the friction coefficient under lubricated conditions. Tribol Lett. 2007;28:131-7.

[24] Suh AY, Lee SC, Polycarpou AA. Adhesion and friction evaluation of textured slider surfaces in ultra-low flying head-disk interfaces. Tribol Lett. 2004;17:739-49.

[25] Davis B, Cusano C. The Tribological Evaluation of Compressor Contacts Lubricated by Oil-Refrigerant Mixtures. 1992.

[26] Suh AY, Patel JJ, Polycarpou AA, Conry TF. Scuffing of cast iron and Al390-T6 materials used in compressor applications. Wear. 2006;260:735-44.

[27] Cannon AH, King WP. Casting metal microstructures from a flexible and reusable mold. Journal of Micromechanics and Microengineering. 2009;19.

[28] Cannon AH, King WP. Microstructured metal molds fabricated via investment casting. Journal of Micromechanics and Microengineering. 2010;20.

[29] Mishra SP, Polycarpou AA. Tribological studies of unpolished laser surface textures under starved lubrication conditions for use in air-conditioning and refrigeration compressors. Tribology International. 2011;44:1890-901.

[30] Han J, Fang LA, Sun JP, Ge SR. Hydrodynamic Lubrication of Microdimple Textured Surface Using Three-Dimensional CFD. Tribol T. 2010;53:860-70.

[31] Dobrica MB, Fillon M, Pascovici MD, Cicone T. Optimizing surface texture for hydrodynamic lubricated contacts using a mass-conserving numerical approach. P I Mech Eng J-J Eng. 2010;224:737-50.

[32] Patankar SV. Numerical heat transfer and fluid flow / Suhas V. Patankar. Washington : New York :: Hemisphere Pub. Corp. ; McGraw-Hill; 1980.

[33] Marian VG, Kilian M, Scholz W. Theoretical and experimental analysis of a partially textured thrust bearing with square dimples. P I Mech Eng J-J Eng. 2007;221:771-8.

[34] Pascovici MD, Cicone T, Fillon M, Dobrica MB. Analytical investigation of a partially textured parallel slider. P I Mech Eng J-J Eng. 2009;223:151-8.

[35] Fowell M, Olver AV, Gosman AD, Spikes HA, Pegg I. Entrainment and inlet suction: Two mechanisms of hydrodynamic lubrication in textured bearings. J Tribol-T Asme. 2007;129:336-47.

[36] Lebeck AO. Principles and Design of Mechanical Face Seals: Wiley-Interscience; 1991.

[37] Brunetière N, Tournerie B. Numerical analysis of a surface-textured mechanical seal operating in mixed lubrication regime. Tribology International. 2012;49:80-9.

[38] Qiu Y, Khonsari MM. Performance Analysis of Full-Film Textured Surfaces With Consideration of Roughness Effects. Journal of Tribology. 2011;133:021704-10.

[39] Ryk G, Kligerman Y, Etsion I. Experimental investigation of laser surface texturing for reciprocating automotive components. Tribol T. 2002;45:444-9.

[40] Pettersson U, Jacobson S. Influence of surface texture on boundary lubricated sliding contacts. Tribol Int. 2003;36:857-64.

[41] Wang XL, Kato K, Adachi K, Aizawa K. Loads carrying capacity map for the surface texture design of SiC thrust bearing sliding in water. Tribol Int. 2003;36:189-97.

[42] Kovalchenko A, Ajayi O, Erdemir A, Fenske G, Etsion I. The effect of laser texturing of steel surfaces and speed-load parameters on the transition of lubrication regime from boundary to hydrodynamic. Tribol T. 2004;47:299-307.

[43] Siripuram RB, Stephens LS. Effect of deterministic asperity geometry on hydrodynamic lubrication. J Tribol-T Asme. 2004;126:527-34.

[44] Braidic-Mitidieri P, Gosman AD, Ioannides E, Spikes HA. CFD analysis of a low friction pocketed pad bearing. J Tribol-T Asme. 2005;127:803-12.

[45] Pettersson U, Jacobson S. Textured surfaces for improved lubrication at high pressure and low sliding speed of roller/piston in hydraulic motors. Tribol Int. 2007;40:355-9.

[46] Qiu Y, Khonsari MM. Experimental investigation of tribological performance of laser textured stainless steel rings. Tribol Int. 2011;44:635-44.

[47] Yamakiri H, Sasaki S, Kurita T, Kasashima N. Effects of laser surface texturing on friction behavior of silicon nitride under lubrication with water. Tribol Int. 2011;44:579-84.

[48] Mitchell N, Eljach C, Lodge B, Sharp JL, DesJardins JD, Kennedy MS. Single and reciprocal friction testing of micropatterned surfaces for orthopedic device design. J Mech Behav Biomed. 2012;7:106-15.

APPENDIX

A.1 Constant clearance applications

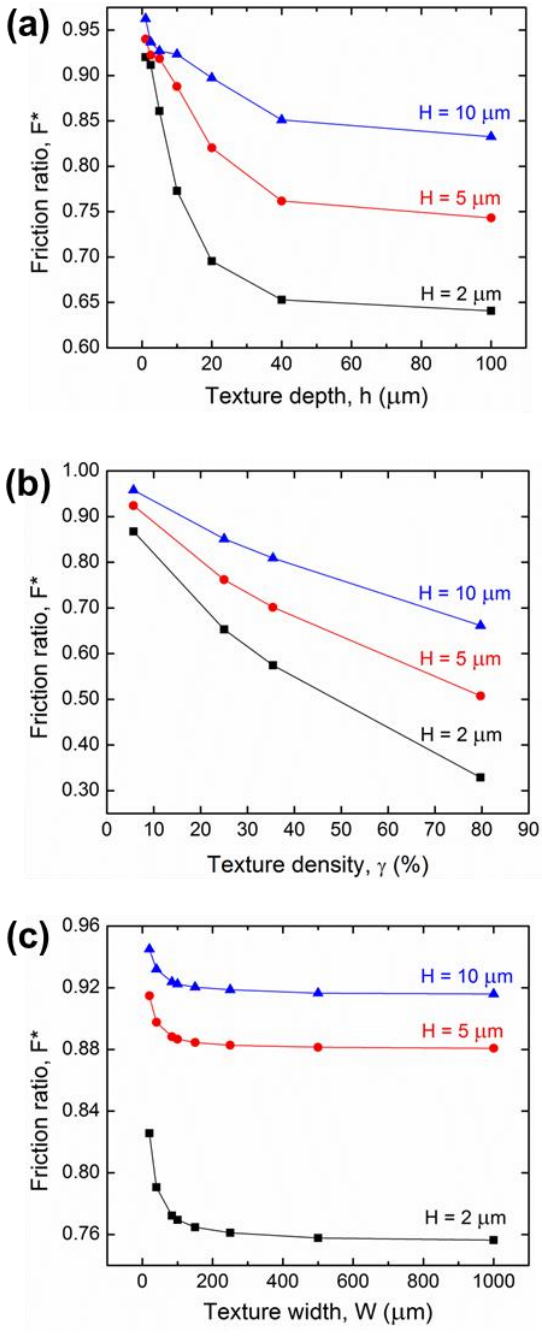

Figure A.1.1: Prediction for friction ratio as a function of texture parameters for u = 0.36 m/s and η = 1.5 Pa-s at constant clearance. (a) Texture depth dependence for texture density γ = 25 % and pitch L = 168 μm. (b) Texture density dependence for texture depth h = 40 μm and pitch L = 168 μm. (c) Texture width dependence for texture depth h = 10 μm and density γ = 25 %.

Figure A.1.1 shows simulation results highlighting how texture depth, width, and density affect the friction ratio at constant clearance. We define the friction ratio F^* as the ratio of the friction force (F) between a textured-untextured surface pair to the friction force (F_{UT}) between untextured-untextured surface pair, $F^* = F/F_{UT}$. Friction ratio decreases with increasing texture depth (Fig. A.1.1a). This is because surface texturing in the form of dimples provides a larger flow path for the fluid compared to untextured surfaces. This translates to an increase in the effective film thickness between the surfaces. In Couette flow, the shear stress is inversely proportional to the film thickness (H) and hence, deeper textures lead to higher friction reduction. Figure A.1.1a also shows that beyond a certain depth when the aspect ratio is greater than unity, the friction force does not reduce. Figure A.1.1c shows the effect of friction ratio on texture width for various film thicknesses. The friction force decreases with increasing texture width. However, beyond a critical width which is about ten times the film thickness, the friction force does not reduce further. To summarize, the texture with width and depth approximately ten times the film thickness and high texture density gives rise to the least friction at constant clearance.

A.2 Leakage studies

There is a tradeoff between friction and leakage in any seal: it is always possible to increase the gap between mating surfaces to decrease friction. However this gap increase also increases leakage. In order to directly compare textured and nontextured surfaces, we define the friction-leakage (F-L) ratio, which is the friction reduction (%) divided by leakage increase (%). When this ratio is greater than one, there is a net benefit. While this ratio is not the key design parameter in a fluid power system, it allows for clear performance comparison between different

surfaces. An example prediction is shown in Fig. A.2.1 for a Couette flow. Such flows are typical of automotive or piston pump applications where the piston moves within a bearing and there is leakage and friction between the piston outer diameter and the bearing. The figure shows the calculated F-L ratio for textured and smooth surfaces when velocity = 12 m/sec, viscosity = 1.5 Pa-sec (gear oil), and the initial film thickness = 20 μm. For the microtextured surface, texture depth = 1-100 μm. When the gap thickness is increased between smooth surfaces, the F-L ratio slightly decreases, illustrating why this is not a preferred approach. When one surface is microtextured, there is a range of textures for which there is a significant benefit in leakage between textured and untextured surfaces for the same friction reduction.

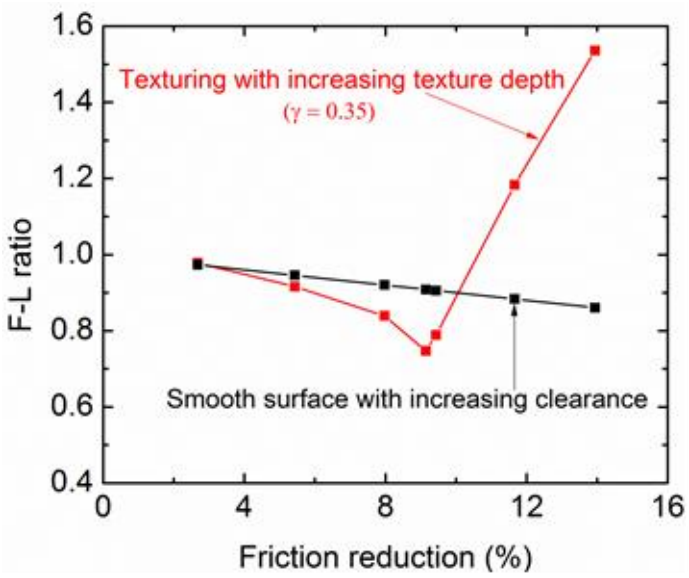

Figure A.2.1: Comparison of the friction and leakage characteristics of smooth and textured surfaces. The F-L ratio is the ratio of friction decrease to leakage increase. For a range of parameters, the microtextured surfaces have clear benefits compared to smooth surfaces.